

Role of relativistic effects and three-body forces in nuclear matter propertiesS. Heidari,¹ S. Zaryouni,^{1,*} H. R. Moshfegh,² and S. Goudarzi²¹*Department of Physics, Bu-Ali Sina University, Hamedan, Iran*²*Department of Physics, University of Tehran, P.O. Box 14395-597, Tehran, Iran*

(Received 4 September 2018; revised manuscript received 20 October 2018; published 11 February 2019)

The role of three-body force (TBF) and the relativistic corrections (RC) on the equations of state of nuclear matter and β -stable matter (BSM) within the relativistic lowest-order constrained variation (RLOCV) approach are studied. The AV14 potential and its relativistic version (\tilde{v}_{14}) as well as the AV18 potential are considered as the bare two-body potentials by employing the nuclear many-body Hamiltonian. It is shown that by using \tilde{v}_{14} , all properties of cold nuclear matter can be correctly reproduced if TBF is used in RLOCV framework. The energy and proton abundance of BSM are calculated for a wide range of baryon number densities, which are of interest in astrophysics. It is also shown that by adding RC or TBF to our calculations, the maximum proton abundance is pushed toward lower densities. Furthermore, the particle number densities decrease by including RC and increase when TBF is added to the interactions. The opposite behaviors for the role TBF and RC on saturation properties of nuclear matter as well as proton number densities of nuclear β -stable matter are found. It is also shown that the effects of three-body forces are much larger than those of relativistic corrections.

DOI: [10.1103/PhysRevC.99.024307](https://doi.org/10.1103/PhysRevC.99.024307)**I. INTRODUCTION**

The equation of state (EOS) of symmetric nuclear matter (SNM) and isospin-asymmetric nuclear matter, especially pure neutron matter (PNM), plays a crucial role in both nuclear physics and its astrophysical applications. The energy-density functional is very important in understanding relativistic heavy-ion collision, neutron stars, stellar collapse, β -stable matter, core-collapse supernova, etc. [1–3]. Moreover, the nuclear matter symmetry energy and its density dependence are important quantities in determining many significant nuclear properties [4], such as the structure of nuclei near the drip line and neutron skin of nuclear systems [5,6]. In addition, the relation between the equation of state of neutron star and its radius and the characterization of core crust transition in neutron stars can put important constraints on the density dependence of symmetry energy [7–9].

The EOS of asymmetric nuclear matter (ANM) that also contains a certain amount of lepton is essential for the interior part of neutron stars [2]. Since the properties of proton and neutron superfluidity in protonneutron stars are related only to the indirect observations, suitable theoretical predictions based on microscopic many-body methods are desirable [10]. Moreover, the density-dependence behavior of the symmetry energy influences strongly on the values of proton fraction and the composition of β -stable nuclear matter [11,12].

During the past few decades, nuclear matter and symmetry energy and its density dependence have been studied within various phenomenological and microscopic many-body approaches based on a variety of phenomenological and mi-

croscopic two-body interactions and phenomenological three-body forces (TBF) in both relativistic and nonrelativistic approaches.

There are some well-known theoretical many-body approaches that one can use to study the EOS of nuclear matter. These approaches can be divided into microscopic and phenomenological ones. In the phenomenological approaches such as Hartree-Fock (HF) [13], Thomas-Fermi (TF) [14], and the mean-field approximation (MF) [15], the parameters of interaction are fixed to nuclear saturation properties, such as saturation density and energy, incompressibility, symmetry energy, and so on.

The microscopic approaches are based on realistic potentials, the parameters of which are fitted to experimental nucleon-nucleon- (NN) scattering data and deuteron properties. Therefore, the EOS obtained from microscopic approaches are more fundamental than those obtained from phenomenological ones, especially in high density of nuclear matter. There are generally two methods of microscopic approaches: Brueckner-type [16] and variational methods. The Fermi hypernetted chain (FHNC) [17], variational Monte Carlo (VMC) [18], and lowest-order constrained variational method (LOCV) [19] are among the well-known variational approaches.

The LOCV method is a self-consistent one which is capable of calculating the properties of various nuclear systems such as symmetric and asymmetric nuclear matter, pure neutron matter, and β -stable matter by using well-defined phenomenological potentials such as Ried [20,21], Urbana V14 (AV14) [17], Argonne V14 (AV14) [22], Argonne V18 (AV18) [23], and \tilde{v}_{14} potentials (which is a fitted relativistically NN -scattering phase shift) [24,25]. This method is also generalized to finite temperature to study the thermodynamic properties of mentioned nucleonic systems [26–28].

*Corresponding author: zaryouni@basu.ac.ir

The LOCV formalism is also extended to the relativistic regime by Moshfegh and Zaryouni [29,30], namely the relativistic lowest-order constrained variational formalism (RLOCV). The RLOCV formalism is based on the works of Bakamjian and Thomas [31] and Krajcik and Foldy [32] in the variational hypernetted chain approach (VHC) [33]. It has been used for nuclear matter at both zero and finite temperatures [29,30,34–36]. It is well known that the many-body approaches are unable to reproduce the correct empirical saturation properties of cold symmetric nuclear matter, i.e., saturation density ($0.17 \pm 0.01 \text{ fm}^{-3}$), binding energy per nucleon ($-16 \pm 1 \text{ MeV}$), and symmetry energy ($31.6 \pm 2.66 \text{ MeV}$) when only two-body interactions are included in the nonrelativistic Hamiltonian. Moreover, adding only the relativistic corrections (RC) to the energies of nuclear matter with a two-body phenomenological potential which has been fitted nonrelativistically to NN -scattering phase shifts cannot solve the nuclear matter problem. In addition, because the relativistic effects can be interpreted as three-body forces (TBF) in the nonrelativistic regimes [37], and because there has been a competition between relativistic and three-body forces effects for a long time, it is of great interest to compare the role of TBF with that of RC in nuclear calculations. The Urbana interaction, which includes attractive and repulsive terms, based on meson exchange theory, has been presented by Carlson, Pandharipande, and Wiringa [38]. The few parameters appearing in these forces are fitted in order to reproduce the empirical saturation density and binding energy of three-body nuclear systems. The phenomenological Urbana-type (UIX) force has been used by Goudarzi and Moshfegh in the LOCV method [39].

Motivated by this fact, we compare the EOS of nuclear matter and density dependence of symmetry energy by a full microscopic many-body calculation in both relativistic and nonrelativistic regimes. We use a realistic potential in our nuclear Hamiltonian, which has been fitted relativistically to NN -scattering data, i.e., v_{14} , and its nonrelativistic version, namely AV14 two-body interaction [22,25,40]. Furthermore, we supplement the Urbana TBF (UIX) [41,42] to these two-body potentials and compare the role of RC and TBF on nuclear matter properties using both potentials [16,24,42,43].

With respect to the above arguments, the purpose of this work is to compare the role of TBF and RC on the nuclear matter properties as well as the BSM using both AV14 interaction and its relativistic version, namely v_{14} , in the LOCV framework at zero temperature. The three-nucleon force is included in the LOCV structure via an effective two-body potential which is driven after averaging out of the third particle, being weighted by the LOCV two-body correlation functions of the 1S_0 channel. The phenomenological Urbana type of the three-body force is employed as an original three-body force. The details are presented in Ref. [37]. Since there is a competition between the TBF and relativistic effects, we have compared the effects of this new version of TBF with RC ones.

The outline of the article is as follows: Some important nuclear matter properties, which we discussed above, are presented in Sec. II. Section III is devoted to β -stable matter. The relativistic contributions are described in Sec. IV. Section V

describes briefly the UIX three-body force model. Finally, the results and conclusions are considered in Sec. VI.

II. NUCLEAR MATTER PROPERTIES

Cold nuclear matter is an ideal system of infinite nucleons which interact by only strong nuclear forces at zero temperature. The energy per particle of cold nuclear matter depends on both baryon density and asymmetric parameter δ defined as $\delta = \frac{1-R}{1+R}$, where R is the ratio of proton to neutron densities. It is clear that R is equal to 1 and zero for SNM and PNM, respectively.

The EOS of SNM can be expanded around the saturation density ρ_0 by neglecting the higher-order terms as the following parabolic approximation:

$$E_0(\rho, \delta = 0) = E_0(\rho_0) + \frac{K_0}{2} \chi^2 + O(\chi^3) + \dots, \quad (1)$$

where $E_0(\rho_0)$ is the binding energy per nucleon at saturation density for SNM, χ is a conventional dimensionless variable that is defined as $\chi = \frac{\rho - \rho_0}{3\rho_0}$, and K_0 is the incompressibility of SNM and describes the curvature of $E(\rho, \delta = 0)$ at saturation density, expressed as:

$$K_0(\delta = 0) = 9\rho_0^2 \left[\frac{d^2 E(\rho, \delta = 0)}{d\rho^2} \right]_{\rho_0}. \quad (2)$$

Obviously, according to the definition of saturation density of SNM, the first power of χ should be absent in Eq. (1). It has been shown that the general accepted range of the isobaric incompressibility of SNM is within the range $230 \pm 40 \text{ MeV}$ [44], and $250 < K_0 < 315 \text{ MeV}$, which is measured from the nuclear giant monopole resonance [45]. One can expand the isobaric incompressibility of asymmetric nuclear matter around asymmetric parameter $\delta = 0$ as:

$$K(\delta) = K_0(\delta = 0) + K_{\text{asy}} \delta^2 + O(\delta^4) + \dots, \quad (3)$$

where K_0 is expressed by Eq. (2) and K_{asy} describes the isospin dependence of the isobaric incompressibility at saturation density.

Moreover, one can expand the energy of asymmetric nuclear matter around the asymmetric parameter $\delta = 0$ at each density as:

$$E(\rho, \delta) = E(\rho, \delta = 0) + \frac{1}{2!} \left[\frac{\partial^2 E(\rho, \delta)}{\partial \delta^2} \right]_{\delta=0} \delta^2 + O(\delta^4) + \dots \quad (4)$$

It is seen that the odd-order terms in δ are absent in Eq. (4), due to the exchange symmetry between neutrons and protons when the Coulomb interaction is neglected. The expansion coefficient in the second term is the general symmetry energy, i.e.,

$$E_{\text{sym}}(\rho)|_{\text{(exact)}} = \frac{1}{2!} \left[\frac{\partial^2 E(\rho, \delta)}{\partial \delta^2} \right]_{\delta=0}. \quad (5)$$

Since the major contribution of symmetry energy is due to the quadratic term (for example, the magnitude of the δ^4) the coefficient at nuclear saturation density has been calculated less than 1 MeV [46]. Neglecting the higher-order terms in

Eq. (4) leads to the famous empirical parabolic law for the asymmetric nuclear matter. Within the parabolic approximation, the density dependence of symmetry energy can be extracted as:

$$E_{\text{sym}}(\rho)|_{\text{(approximate)}} = E(\rho, \delta = 1) - E(\rho, \delta = 0), \quad (6)$$

Moreover, the nuclear symmetry energy can be expanded around the nuclear saturation density. Up to the second order of χ , it is expressed as:

$$E_{\text{sym}}(\rho) = E_{\text{sym}}(\rho_0) + L\chi + \frac{K_{\text{sym}}}{2!}\chi^2 + \dots, \quad (7)$$

in which L and K_{sym} denote the slope and curvature parameters of symmetry energy around ρ_0 defined as:

$$L = 3\rho_0 \left[\frac{dE_{\text{sym}}(\rho)}{d\rho} \right]_{\rho_0}, \quad K_{\text{sym}} = 9\rho_0^2 \left[\frac{d^2E_{\text{sym}}(\rho)}{d\rho^2} \right]_{\rho_0}, \quad (8)$$

If the parabolic approximation of EOS of SNM is used, i.e., Eq. (1), then K_{asy} can be expressed as:

$$K_{\text{asy}} \simeq K_{\text{sym}} - 6L. \quad (9)$$

The quantities $E_0(\rho_0)$, K_0 , $E_{\text{sym}}(\rho_0)$, L , and K_{sym} provide reliable information about nuclear properties and isospin dependence of nuclear symmetry energy.

III. β -STABLE MATTER

β -stable matter is an equilibrium mixture of protons, neutrons, and a certain amount of leptons (electrons and muons) that is electrically neutral. The nucleons interact through strong forces, and the condition of charge neutrality states where the electromagnetic interaction can be ignored and the weak interactions are neglected.

The baryon number density (ρ_B) is expressed as the sum of neutron and proton number densities,

$$\rho_B = \rho_n + \rho_p, \quad (10)$$

and the condition of electrical neutrality requires:

$$\rho_p = \rho_e + \rho_\mu, \quad (11)$$

where ρ_e and ρ_μ are the electron and muon number densities, respectively.

The leptons (electrons and muons) form two relativistic Fermi seas. The contribution of the energy per baryon of these Fermi seas is [47]

$$E_L = \sum_{i=e,\mu} \frac{m_i^4 c^5}{8\pi^2 \hbar^3 \rho_B} [x_i(1+x_i^2)^{1/2}(2x_i^2+1) - \sinh^{-1}x_i], \quad (12)$$

where

$$x_i = \hbar k_i / m_i c, \quad (13)$$

where $k_e(k_\mu)$ are the electron (muon) Fermi momenta. These Fermi momenta are related through the chemical equilibrium condition of β stability, i.e.,

$$\mu_n - \mu_p = \mu_e = \mu_\mu, \quad (14)$$

where μ states the chemical potential of particle. This condition implies that

$$m_e c^2 (1+x_e^2)^{1/2} = m_\mu c^2 (1+x_\mu^2)^{1/2}. \quad (15)$$

To calculate the chemical potentials of neutrons and protons, one need to know the EOS of asymmetrical nuclear matter. It can be shown that if the asymmetry dependence of is EOS assumed to be quadratic, i.e., approximate Eq. (4) up to the second term, then we can find $\mu_n - \mu_p = 4E_{\text{sym}}(\rho)\delta$. Then the role of symmetry energy is obvious. Thus, the energy per nucleon for β -stable matter is

$$E = \sum_{i=p,n} \frac{\rho_i}{\rho_B} \left(\frac{3}{5} \frac{\hbar^2}{2m_i} k_i^2 + m_i c^2 \right) + E_L + E_2, \quad (16)$$

where $k_p(k_n)$ are the proton (neutron) Fermi momenta and E_2 is the two-body cluster energy. By minimizing E with respect to the correlation functions under the constraints of Eqs. (10), (11), and (14), the proton abundance ρ_p/ρ_B can be obtained at each baryon number density.

IV. RELATIVISTIC CONTRIBUTION

The relativistic Hamiltonian, reported by Bakamjian and Thomas [31] and Krajcik and Foldy [9,32] in a relativistically covariant form, can be written as:

$$H_R = \sum_i^N [\sqrt{p_i^2 c^2 + m_i^2 c^4} - m_i c^2] + \sum_{i<j} [\tilde{v}_{ij} + \delta v(P_{ij})], \quad (17)$$

where \tilde{v}_{ij} is the two-body potential which is determined by fitting deuteron properties and two nucleon scattering data by using the relativistic quantum mechanics in the two-body rest frame in which their total momentum ($P_{ij} = p_i + p_j$) vanishes [24,34] and can be written as:

$$\tilde{v}(12) = \sum_{p,\alpha} V_\alpha^p(12) O_\alpha^p, \quad (18)$$

where $V_\alpha^p(12)$ is the two-nucleon interaction in each channel and $\alpha = \{J, L, S, T, M_T\}$; $p = 1$ is used for uncoupled channels (singlet and triplet channels with $J = L$) and $p = 2, 3$ are used for triplet channels with $J = L \pm 1$. $O_\alpha^{p=1,2,3}$ are given by [19,48]:

$$O_\alpha^{p=1,2,3} = 1, (2/3) + (1/6)S_{12}, (1/3) - (1/6)S_{12}, \quad (19)$$

where $S_{12} = 3(\sigma_1 \cdot \hat{r})(\sigma_2 \cdot \hat{r}) - (\sigma_1 \cdot \sigma_2)$ is the usual tensor operator.

Moreover, $\delta v(P_{ij})$ in Eq. (1) is called the boost interaction. As mentioned in our previous works, it depends on the total momentum of interacting particles [24,34]. It is obvious that:

$$\delta v_{ij}(P_{ij} = 0) = 0. \quad (20)$$

Krajcik and Foldy [32] formally calculated $\delta v(P_{ij})$ to all orders in $\frac{P_{ij}^2}{4(mc)^2}$. In our calculations, as well as Friar, Forest, and Pandharipande [9,49], we keep only the first two terms of

$\delta v(P_{ij})$ [34,35] related to the static parts of v_{ij} , i.e.,

$$\delta v(P_{ij}) = -\frac{P_{ij}^2}{8(mc)^2} v_{ij}^s + \frac{1}{8(mc)^2} [P_{ij} \cdot r_{ij} P_{ij} \cdot \nabla_{ij}, v_{ij}^s]. \quad (21)$$

where v_{ij}^s represents the static part of potential. The two terms are denoted by δv^{RE} and δv^{LC} , the relativistic energy expression and Lorentz contraction of boost interaction corrections, respectively. The derived relations of δv^{RE} and δv^{LC} are reported in Refs. [35].

In LOCV formalism, the trial wave function in many-particle interacting systems is denoted by [19,26–28,30,36,50]:

$$\psi = \mathcal{F}\varphi, \quad (22)$$

where φ is a Slater determinant of single-particle state wave functions of N independent nucleons (ideal Fermi gas wave function) and \mathcal{F} 's are the N -body correlation functions which can be given by the product of the two-body correlation functions in Jastrow form, written as

$$\varphi = \mathcal{A} \prod_{i=1}^N \phi_i, \quad (23)$$

$$\mathcal{F} = \mathcal{S} \prod_{i<j} f(ij), \quad (24)$$

where ϕ_i 's are one-body wave functions, $\mathcal{A}(\mathcal{S})$ is an anti-symmetric (symmetric) operator, and $f(ij)$'s are two-body correlation functions that are written as:

$$f(ij) = \sum_{\alpha,p} f_{\alpha}^{(p)}(ij) O_{\alpha}^{(p)}(ij), \quad (25)$$

in which $O_{\alpha}^{(p)}$ are given by Eq. (19).

Now the energy expectation value per nucleon is obtained in the cluster expansion theory by using the relativistic Hamiltonian [Eq. (17)] and trial wave function [Eq. (22)]. If the contribution of higher-order terms is neglected, then it can be written as:

$$E = \frac{1}{N} \frac{\langle \psi | H_R | \psi \rangle}{\langle \psi | \psi \rangle} = E_{1R} + E_{2R} + \dots, \quad (26)$$

where E_{1R} is one-body kinetic energy in the relativistic lowest-order constrained variation framework for asymmetric nuclear matter which contains Z protons and N neutrons and is independent of $f(ij)$, and can be written as

$$E_{1R} = E_{1NR} + \delta E_{1R}, \quad (27)$$

in which E_{1NR} and δE_{1R} are the nonrelativistic one-body kinetic energy and the relativistic correction of one-body kinetic energy, respectively calculated as [29,34,35]:

$$E_{1NR} = \sum_{i=1}^2 \left(\frac{\rho_i}{\rho_B} \right) \frac{3}{5} \frac{\hbar^2 k_F^i{}^2}{2m}, \quad (28)$$

$$\delta E_{1R} = \left(-\frac{9\pi^2}{7\rho_B} \right) \sum_{i=1}^2 C_R^i k_F^i \rho_i^2, \quad (29)$$

where $\rho_B = \rho_p + \rho_n$ is the baryon density; $C_R^i = \hbar^4/8m_i^3 c^2$; labels 1 and 2 denote protons and neutrons, respectively; and k_F^i is the Fermi momentum of the i th particle and is given by:

$$k_F^i = (3\pi^2 \rho_i)^{1/3}. \quad (30)$$

Also E_{2R} in Eq. (26) is the two-body clusters energy calculated as:

$$E_{2R} = \frac{1}{2A} \sum \langle ij | W_R(12) | ij \rangle_a = E_{2NR} + \delta E_{2R}. \quad (31)$$

In the rest frame, the ‘‘effective potential’’ $W_R(12)$ can be written as:

$$W_R = W_{NR} + \delta W_R, \quad (32)$$

where W_{NR} is defined as

$$W_{NR}(12) = -\frac{\hbar^2}{2m} [f(12), [\nabla_{12}^2, f(12)]] + f(12)V(12)f(12). \quad (33)$$

and δW_R is obtained to be

$$\begin{aligned} \delta W_R = C_R & (2[\nabla_{12}^2, f(12)][\nabla_{12}^2, f(12)] \\ & - [f(12), [\nabla_{12}^2, f(12)]] \nabla_{12}^2 \\ & - \nabla_{12}^2 [f(12), [\nabla_{12}^2, f(12)]]). \end{aligned} \quad (34)$$

By substituting W_R in Eq. (31) and after some tedious algebraic calculations, Euler-Lagrange equations are obtained by minimizing the two-body cluster energy with respect to variations in the correlation functions under normalization constraint. By solving these equations, δE_{2R} can be calculated. An explicit relation for δE_{2R} is stated in Ref. [35].

V. TBF CONTRIBUTION

As mentioned in the Introduction, the contribution of TBF in the energy of nuclear matter is very important and should be calculated. Therefore, UIX three-body force interaction is included in our Hamiltonian for the purpose of reproducing the correct saturation properties of cold SNM. We use the general form of semiphenomenological UIX interaction, which is based on meson-exchange theory, generally written as

$$V_{123} = V_{123}^{2\pi} + V_{123}^R, \quad (35)$$

where $V_{123}^{2\pi}$ and V_{123}^R are the contributions of the two-pion exchange potential and the phenomenological repulsive part, respectively, represented as

$$\begin{aligned} V_{123}^{2\pi} = A & \sum_{\text{cyc}} (\{X_{12}, X_{23}\} \{\tau_1 \cdot \tau_2, \tau_2 \cdot \tau_3\} \\ & + \frac{1}{4} [X_{12}, X_{23}] [\tau_1 \cdot \tau_2, \tau_2 \cdot \tau_3]) \end{aligned} \quad (36)$$

and

$$V_{123}^R = U \sum_{\text{cyc}} T(m_{\pi} r_{12})^2 T(m_{\pi} r_{23})^2, \quad (37)$$

where the one-pion exchange operator X_{12} is defined as

$$X_{12} = Y(m_{\pi} r_{12}) \sigma_1 \cdot \sigma_2 + T(m_{\pi} r_{12}) S_{12}, \quad (38)$$

where m_π , σ , τ , and S_{12} are the average pion mass, spin, isospin, and the usual tensor operator, respectively. The indices 1, 2, and 3 refer to three interacting nucleons while adjustable parameters $U = -0.000483$ MeV and $A = -0.0316$ MeV have been determined by Goudarzi and Moshfegh [37] by fitting empirical saturation properties of cold SNM in the LOCV method. $Y(m_\pi r_{12})$ and $T(m_\pi r_{12})$ are the Yukawa and tensor functions, respectively. They are written as

$$Y(m_\pi r_{12}) = \frac{e^{-m_\pi r}}{m_\pi r} (1 - e^{-cr^2}), \quad (39)$$

$$T(m_\pi r_{12}) = \left[1 + \frac{3}{m_\pi r} + \frac{3}{(m_\pi r)^2} \right] \frac{e^{-m_\pi r}}{m_\pi r} (1 - e^{-cr^2})^2. \quad (40)$$

By averaging over the third particle coordinates, and also after being weighted by LOCV calculations, two-nucleon

correlation functions $f(r)$, an effective two-body interaction $\tilde{V}_{12}(r)$ has been derived as a reduced TBF [37] at each density,

$$\tilde{V}_{12}(r) = \rho \int d^3 r_3 \sum_{\sigma_3, \tau_3} f^2(r_{13}) f^2(r_{23}) V_{123}. \quad (41)$$

By inserting Eq. (35) in the above equation and taking the z axis along the vector r_{12} , the effective two-body potential which has the following operator structure is obtained as [37]:

$$\begin{aligned} \tilde{V}_{12}(r) = & (\tau_1 \cdot \tau_2)(\sigma_1 \cdot \sigma_2) V_{\sigma\tau}^{2\pi}(r) \\ & + S_{12}(\hat{r})(\tau_1 \cdot \tau_2) V_t^{2\pi}(r) + V_c^R(r), \end{aligned} \quad (42)$$

where

$$V_{\sigma\tau}^{2\pi}(r) = \frac{2\pi}{r} \rho \int_0^\infty x dx \int_{|r-x|}^{|r+x|} y dy f^2(x) f^2(y) \sum_{\text{cyc}} \sum_{\sigma_3 \tau_3} 4A [Y(m_\pi x) Y(m_\pi y) + 2P_2(\cos\theta) T(m_\pi x) T(m_\pi y)], \quad (43)$$

$$\begin{aligned} V_t^{2\pi}(r) = & \frac{2\pi}{r} \rho \int_0^\infty x dx \int_{|r-x|}^{|r+x|} y dy f^2(x) f^2(y) \sum_{\text{cyc}} \sum_{\sigma_3 \tau_3} 4A [Y(m_\pi x) T(m_\pi y) P_2(\cos\theta_x) \\ & + T(m_\pi x) Y(m_\pi y) P_2(\cos\theta_y) + T(m_\pi x) T(m_\pi y) P], \end{aligned} \quad (44)$$

$$V_c^R(r) = \frac{2\pi}{r} \rho \int_0^\infty x dx \int_{|r-x|}^{|r+x|} y dy f^2(x) f^2(y) \times \sum_{\text{cyc}} \sum_{\sigma_3 \tau_3} U [T(m_\pi x) T(m_\pi y)]^2. \quad (45)$$

The details and notations of Eqs. (43) to (45) are described in Ref. [37]. In the next section we present our results regarding the effects of both TBF and RC on the saturation properties of SNM, the symmetry energy of our nuclear matter and β -stable matter with the LOCV, as well as the RLOCV methods by using two different potentials AV14 and its relativistic version, i.e., \tilde{v}_{14} , obtained relativistically NN -scattering phase shift.

VI. RESULTS AND DISCUSSION

First, we consider the results which are obtained for symmetric nuclear matter. The next subsection is devoted to the calculation of asymmetric nuclear matter. Finally, the results of β -stable matter are given in the last subsection.

A. Symmetric nuclear matter

As mentioned in the previous section, we use the relativistic model of \tilde{v}_{14} which was introduced by Carlson, Pandharipande, and Schiavilla [24,25] to present our numerical results for nuclear matter. This potential is a two-body phenomenological interaction in configuration space that has been relativistically fitted with the NN -scattering data. We have compared the results of the effects of TBF and RC which come from this potential and its nonrelativistic version, i.e., the AV14 potential.

We start with presenting the results of EOS of SNM. Figure 1 shows the density dependence of energy per nucleon

of SNM for two-body potentials, i.e., AV14 and \tilde{v}_{14} as well as both potentials which were supplemented by the TBF of the Urbana UIX interaction, i.e., AV14+UIX and \tilde{v}_{14} +UIX in the LOCV and RLOCV formalisms. It is seen that the binding energy decreases and the saturation density increases by including RC, i.e., $\delta E_R + \delta v$ ($\delta E_R = \delta E_{1R} + \delta E_{2R}$) to the nuclear Hamiltonian, especially for both 2BF interactions AV14 and \tilde{v}_{14} and not so much for 2BF+TBF potentials AV14+UIX and \tilde{v}_{14} +UIX. Therefore, as mentioned earlier in Ref. [30], the RC shows a repulsive effect on the EOS of SNM. The same behavior has been reported in Refs. [33,39]. In other words, adding RC to the nuclear Hamiltonian shifts the saturation density toward higher densities and also shifts the binding energy toward the more negative values. On the other hand, the binding energy and the saturation density decrease by adding TBF to both two-body interactions, i.e., AV14 and its relativistic version, \tilde{v}_{14} , in both the LOCV and RLOCV formalisms. Accordingly, the saturation density moves to lower densities and the EOS of SNM becomes harder by including TBF to the nuclear Hamiltonian. Thus TBF shows an attractive effect to the EOS of SNM. Similar results have been observed in the Brueckner-Hartree-Fock (BHF) and LOCV methods with AV18 interaction [8,30,50]. It is seen from this figure that the role of TBF effect on both two-body potentials (relativistic and nonrelativistic ones) is the same in both relativistic and nonrelativistic frameworks, i.e., the RLOCV and LOCV methods. Also, the effect of TBF is more considerable than the effect of RC. In all cases, the relativistic version of the interaction gives stiffer EOS than the

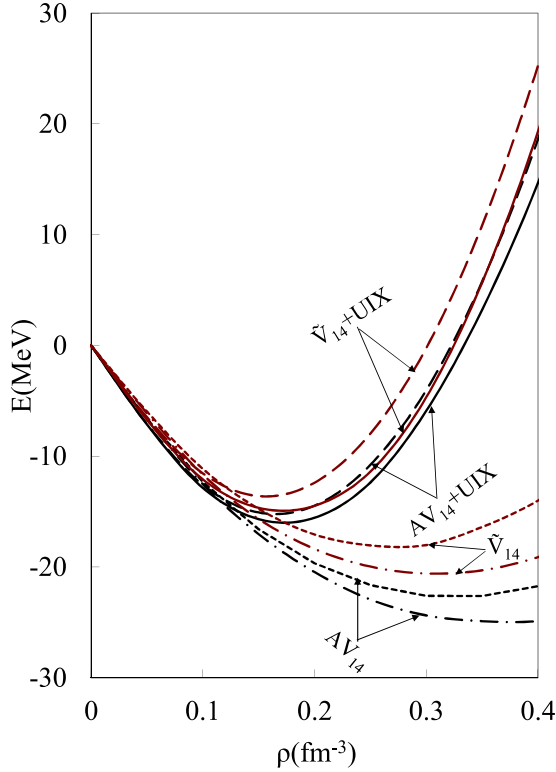


FIG. 1. The binding energy per nucleon versus density for AV_{14} as well as \tilde{v}_{14} . Dot curves are drawn by using H_{NR} in LOCV method without including TBF, dot-dashed curves by using H_R in RLOCV method only by using two-body force (2BF), dashed curves are used for both 2BF and TBF in our LOCV calculations, and solid curves are related to RLOCV method with including TBF to their two-body interactions.

nonrelativistic one. It is due to the fact that the tensor force in \tilde{v}_{14} is weaker than the nonrelativistic one and, consequently, its central component is stronger than AV_{14} . So \tilde{v}_{14} gives rise the binding energy of nuclear matter. The major difference in the strength of the tensor force in nuclear matter arises from the spin triplet isospin singlet 3S_1 - 3D_1 channel. A similar description has been reported in Ref. [24].

Saturation properties of our nuclear matter in LOCV and RLOCV calculations by using 2BF as well as 2BF+TBF and the comparison with other methods and various interactions are listed in Table I. One can see from this table that if two-body interaction $AV_{14}(\tilde{v}_{14})$ is used, then the binding energy is obtained -22.7 (-18.0) MeV at saturation density 0.33 (0.26) fm^{-3} in LOCV formalism, while the result in relativistic regime is -24.9 (-20.6) MeV at 0.37 (0.31) fm^{-3} . Therefore, the saturation point of SNM for both version of two-body interactions gets away from the empirical value by adding the relativistic effects ($\delta E_R + \delta v$) to the EOS of nuclear matter. However, if the two-body relativistic version \tilde{v}_{14} is considered in relativistic nuclear Hamiltonian which is defined by Eq. (17) in RLOCV formalism, then the effects of complete RC means (using relativistic Hamiltonian H_R with relativistic NN interaction) pulls it toward lower values. So it can produce a better saturation point compared with

AV_{14} , but it is still far from the empirical value. Also, if TBF is considered in $AV_{14}(\tilde{v}_{14})$ interaction, using nonrelativistic Hamiltonian in LOCV framework, then the calculated saturation point is -15.2 (13.6) MeV at 0.17 (0.16) fm^{-3} . Therefore, the calculated saturation points (especially saturation densities) by using both relativistic and nonrelativistic versions of potential get close to each other in the RLOCV framework if TBF effects are considered. Moreover, the saturation points by adding TBF to these potentials will get closer to each other and also to empirical values in the RLOCV formalism, i.e., -16.0 (-14.9) MeV at 0.17 (0.17) fm^{-3} . Therefore, the effects of TBF and RC can reproduce the acceptable saturation point in both versions of interaction. So although the relativistic effects alone cannot make the empirical saturation point properly, the TBF effects, especially in the relativistic regime, reproduce the empirical binding energy -16 ± 1 MeV at saturation density 0.17 ± 0.01 fm^{-3} . In addition, the incompressibility of SNM at normal density (K_0), which is calculated by Eq. (2) in both the LOCV and RLOCV methods with two-body interactions AV_{14} , lie neither in the acceptable range 230 ± 40 MeV [44] nor in $250 < K_0 < 315$ MeV, which is obtained by reanalyzing data on the nuclear giant monopole resonance [45], while the isobaric incompressibility with \tilde{v}_{14} lies in the acceptable ranges 230 ± 40 MeV in LOCV or $250 < K_0 < 315$ MeV in the RLOCV framework. On the other hand, the similar calculations by adding TBF to our two-body potentials show that the incompressibility in the LOCV formalism fits in the region $250 < K_0 < 315$ MeV for both versions of interaction, but in the RLOCV method, only the relativistic version of potential fits in the empirical region. Therefore, only in the RLOCV method, by adding TBF to the relativistic potential \tilde{v}_{14} , binding energy, saturation density, and incompressibility lie in the experimental region.

The contribution of the total RC which is given by the sum of one-body and two-body relativistic kinetic energy corrections and the boost interaction corrections, i.e., $\delta E_{RC} = \delta E_R + \delta v$ are listed in Table II for both two-body AV_{14} and \tilde{v}_{14} interactions as well as their 2BF+TBF potentials, i.e., $AV_{14}+UIX$ and $\tilde{v}_{14}+UIX$. As expected, it is seen that RC contributions for \tilde{v}_{14} interaction is more than its nonrelativistic version for all densities.

Since these potentials have been obtained from scattering phase shift, a potential containing a weak tensor component needs a strong central component. So \tilde{v}_{14} has a stronger central component and, consequently, the contribution of RC in \tilde{v}_{14} is higher than its nonrelativistic version. Engvik *et al.* have given the similar report [51]. In addition, the central channel 1S_0 with ($L = 0$) has the largest contribution of relativistic effects, as one can see from Table IV. Similar results are obtained for $\tilde{v}_{14}+UIX$ as compared with $AV_{14}+UIX$ from Table II. It is also obvious from this table that the contribution of RC for both 2BF+TBF interactions, namely $AV_{14}+UIX$ and $\tilde{v}_{14}+UIX$, are higher compared to 2BF potentials AV_{14} and \tilde{v}_{14} , respectively.

As previously mentioned, in order to use TBF in the LOCV formalism, we have averaged over the third particle coordinates to reach a density-dependent effective two-body interaction [37]. Thus, in the LOCV formalism, three-body forces contribute only to the two-body cluster energy. The

TABLE I. A comparison of saturation properties of nuclear matter for LOCV and RLOCV treatment with several many-body interactions and techniques.

Potential	Method	Author	ρ_0 (fm ⁻³)	$E_0(\rho_0)$ (MeV)	$\mathcal{K}(\rho_0)$ (MeV)
AV18	LOCV	GM [37]	0.327	-23.37	373.3
AV18+UIX	LOCV	GMH [50]	0.172	-15.64	306.4
AV18	VHC	APR [33]	0.3	-18.22	289
AV18+UIX	VHC	APR [33]	0.17	-11.9	289
AV18	BHF	VPPR [8]	0.240	-17.30	213.6
AV18+UIX	BHF	VPPR [8]	0.176	-14.62	185.9
UV14	VHC	WFF [64]	0.33	-17.1	243
UV14+TNI	VHC	WFF [64]	0.16	-16.6	261
AV14	VHC	WFF [64]	0.32	-15.6	205
AV14+UIX	VHC	WFF [64]	0.194	-12.4	209
AV18	BHF	ZLLM [65]	0.26	-18.2	207
Bonn	DBHF	DFP [66]	0.193	-16.9	289
AV14	LOCV	This work	0.33	-22.7	354
AV14+UIX	LOCV	This work	0.17	-15.2	303
AV14	RLOCV	This work	0.37	-24.9	316
AV14+UIX	RLOCV	This work	0.17	-16.0	339
\tilde{v}_{14}	LOCV	This work	0.26	-18.0	246
\tilde{v}_{14} +UIX	LOCV	This work	0.16	-13.6	286
\tilde{v}_{14}	RLOCV	This work	0.31	-20.6	304
\tilde{v}_{14} +UIX	RLOCV	This work	0.17	-14.9	283
Empirical			0.17 ± 0.01	-16 ± 1	190–315

contribution of TBF can be considered as $\delta E_{\text{TBF}} = E_2(2BF + TBF) - E_2(2BF)$. We have compared the contribution of TBF for these two kinds of potentials at different densities in Table III. It is seen that the TBF contribution in relativistic version of potential, namely \tilde{v}_{14} , is less than the nonrelativistic one (AV14) for all densities. It can be valuable to determine the separate contributions of RC as well as TBF in different partial waves in our calculation for SNM. Our results of such separation at empirical saturation density 0.17 fm^{-3} have been reported in Table IV. The first two columns present the contributions of TBF and the next two columns show the contributions of RC. It can be seen from Table IV that the 3S_1 - 3D_1 channel gives the significant contribution to TBF, while the 1S_0 channel gives, relatively, the major contribution to RC for both versions of interaction. Similar results have been obtained for all densities. This is due to effect of tensor component of the nuclear force which comes mainly through 3S_1 - 3D_1 channel. The similar explanation has been stated in Refs. [30,52]

 TABLE II. The contributions of RC ($\delta E_{\text{RC}} = \delta E_R + \delta v$) in MeV for symmetric nuclear matter with AV14, \tilde{v}_{14} , AV14+UIX, and \tilde{v}_{14} +UIX interactions.

ρ (fm ⁻³)	AV14	\tilde{v}_{14}	AV14+UIX	\tilde{v}_{14} +UIX
0.1	-0.20	-0.50	-0.31	-0.71
0.15	-0.45	-0.87	-0.61	-1.38
0.2	-0.80	-1.34	-1.00	-2.18
0.25	-1.30	-1.94	-1.48	-3.07
0.3	-1.77	-2.69	-2.06	-4.07
0.35	-2.27	-3.64	-2.78	-5.15
0.4	-3.16	-4.83	-3.66	-6.31

B. Asymmetric nuclear matter

We have calculated the binding energy per nucleon of asymmetric nuclear matter for various values of asymmetric proton to neutron ratio R with step of 0.3, against density for both 2BF potentials, namely AV14, \tilde{v}_{14} as well as their 2BF+TBF potentials, i.e., AV14+UIX and \tilde{v}_{14} +UIX in both the LOCV and RLOCV methods. Our results are presented in Figs. 2(a)–2(d). It is seen from these figures that the difference between two versions of potentials is negligible at low densities and becomes more considerable by increasing density. Moreover, this difference is larger in the LOCV method in comparison with the RLOCV method. Also, this difference is remarkable by employing just 2BF interactions. As expected, including RC in our Hamiltonian pulls the saturation densities toward higher values by decreasing binding energies for different values of R in both interactions, while adding TBF pushes saturation densities toward lower values by increasing binding energies, for various values of

 TABLE III. The contributions of TBF [$\delta E_{\text{TBF}} = E_2(2BF + TBF) - E_2(2BF)$] in MeV for symmetric nuclear matter with AV14 and \tilde{v}_{14} interactions.

ρ	AV14	\tilde{v}_{14}
0.1	-0.27	-0.39
0.15	1.51	1.20
0.2	5.19	4.64
0.25	10.86	10.07
0.3	18.57	17.65
0.35	28.38	27.50
0.4	40.34	39.54

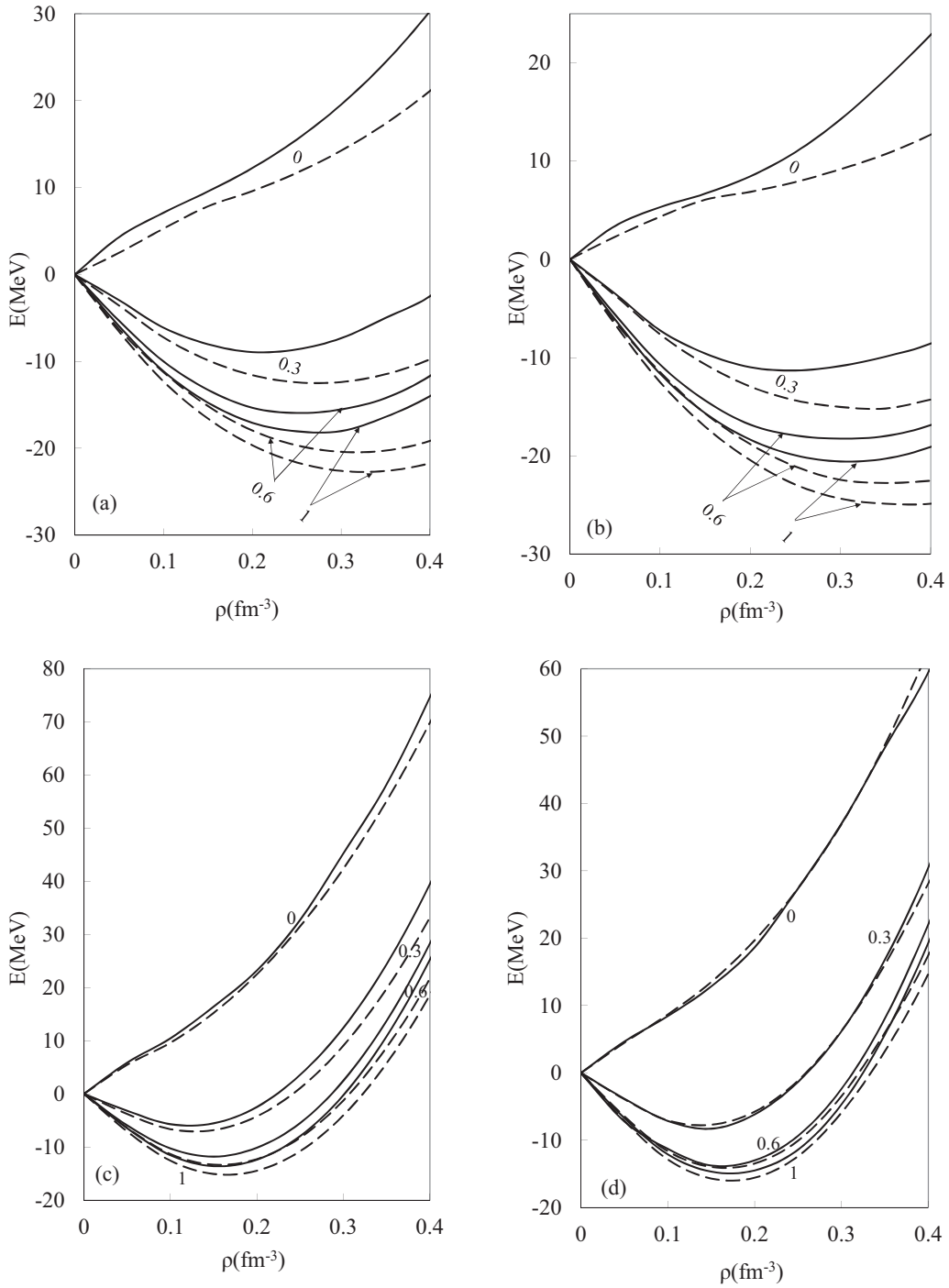


FIG. 2. The comparison of asymmetric nuclear matter binding energy against density for various proton to neutron ratio for both versions of interactions, i.e., AV_{14} (dashed curves) and \tilde{v}_{14} (solid curves). Panels (a) and (b) show the results of 2BF potentials in LOCV and RLOCV calculations, respectively, and panels (c) and (d) are devoted to the results of 2BF+TBF potentials in LOCV and RLOCV methods, respectively.

R in both versions of interactions. On the other hand, at a constant density, when the proton number is decreased, the saturation density leads to lower values and the EOS becomes harder in all cases [Figs. 2(a)–2(d)]. Furthermore, at a constant R , the EOS of \tilde{v}_{14} shows a harder behavior compared with nonrelativistic version AV_{14} whether 2BF or 2BF+TBF interactions are considered, whether the LOCV or RLOCV calculations are regarded. But if both TBF and

RC are added to system Hamiltonian, then the EOS of AV_{14} become very close to its relativistic version, i.e., \tilde{v}_{14} . The proton to neutron ratio that the system becomes no longer bound is 0.08 (0.11) for AV_{14} (\tilde{v}_{14}) in the LOCV calculation, and 0.06 (0.09) in the RLOCV calculation. The calculated mentioned ratio for $AV_{14}+UIX$ ($\tilde{v}_{14}+UIX$) is 0.14 (0.15) in the LOCV calculation, and 0.13 (0.13) in the RLOCV calculation, too. Therefore, in our relativistic calculation, if TBF

TABLE IV. The separate contributions of δE_{TBF} as well as δE_{RC} of partial waves in MeV for SNM with AV14 and \tilde{v}_{14} interactions at saturation density 0.17 fm^{-3} . All the quantities are in MeV.

Partial waves	TBF	TBF	RC	RC
	AV14	\tilde{v}_{14}	AV14	\tilde{v}_{14}
1S_0	1.12	1.00	-0.70	-0.96
3P_0	0.17	0.17	-0.02	-0.06
1P_1	2.04	2.04	-0.05	-0.04
3S_1 - 3D_1	-3.82	-3.82	0.53	0.03
3P_1	0.40	0.42	0.001	-0.04
1D_2	-0.04	-0.04	0.03	0.03
3D_2	1.44	1.41	-0.006	-0.005
3P_2 - 3F_2	0.32	0.32	-0.02	0.0080

includes in potentials, then the proton-to-neutron ratio that the system becomes no longer bound is the same for two different versions of interaction. Apparently, the effective potential wall of relativistic version of interaction (\tilde{v}_{14}) is shallower than nonrelativistic one (AV14) as the system moves to PNM. Also, the effect of RC causes this effective potential wall to become deeper, while the effects of TBF is inverse. The effect of both RC and TBF cause the depth of this potential wall for both versions of interaction to become similar. Our results

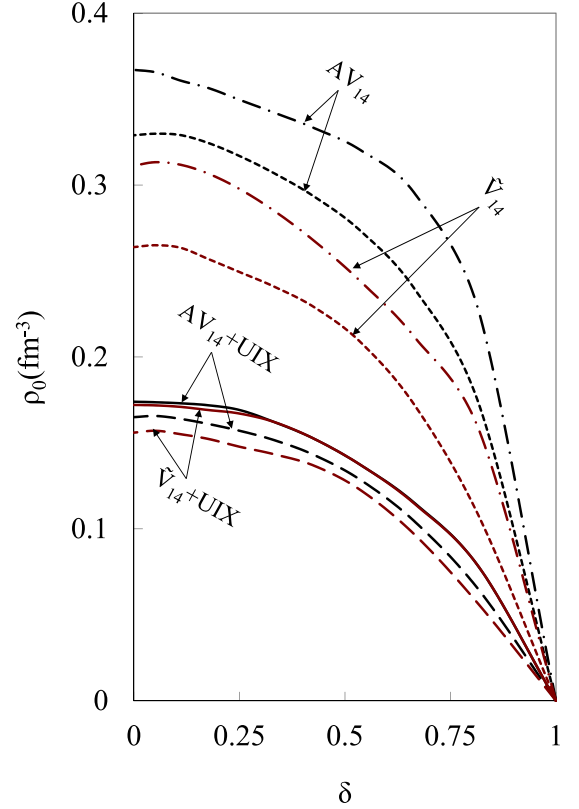


FIG. 4. The same as Fig. 3 but for the saturation density of nuclear matter.

are comparable with the BHF and DBHF methods [53–55], the LOCV formalism with Reid 93 [28], as well as the TF approach [56,57].

In Fig. 3 the asymmetric nuclear matter saturation energy has been plotted against the asymmetry parameter δ in both the LOCV and RLOCV calculations, respectively. In all cases the absolute value of saturation energy in the relativistic version of interaction is less than the nonrelativistic one. Moreover, these values are different at asymmetric systems, and this difference decreases by increasing the asymmetric parameter δ . It is also seen from this figure when TBF is added to both versions of potentials specially in relativistic approach, the values of saturation energies come close to each other. The similar comparison has been presented for the saturation density versus δ in Fig. 4. It is observed that our interactions decreases saturation density while, including RC to our calculations increases ρ_0 . It seems the effects of RC and TBF are completely different on nuclear matter. The effect of TBF is also significant in compared with RC. Moreover, the effect of TBF on saturation density is more considerable than the effect of TBF on binding energy.

The nuclear symmetry energy of asymmetric nuclear matter can be obtained from Eq. (6) with a good parabolic approximation. Figure 5 shows the quadratic dependence of symmetry energy as a function of quadratic isospin asymmetry parameter (δ^2) for both versions of 2BF potentials (AV14 and \tilde{v}_{14}) as well as 2BF+TBF potentials AV14+UIX,

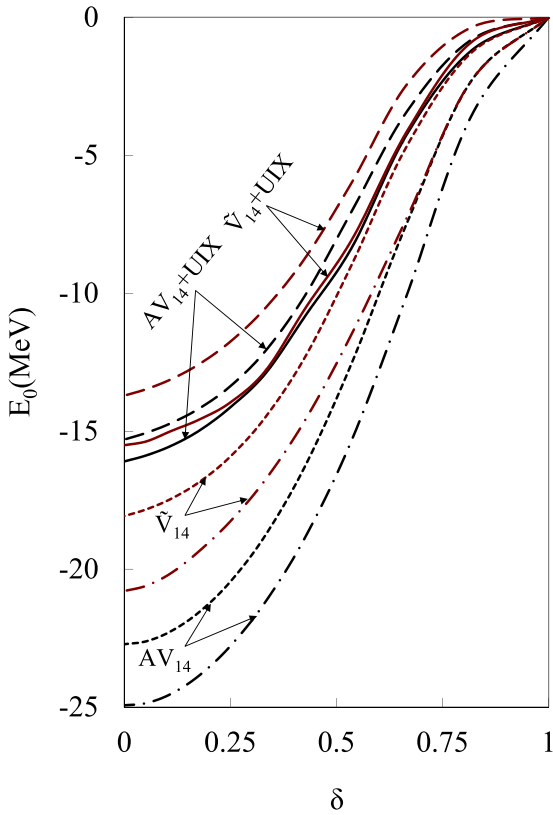


FIG. 3. The comparison of the saturation energy per nucleon versus asymmetry parameter for both 2BF interactions AV14 and \tilde{v}_{14} in LOCV method (dot curves), in RLOCV method (dot-dashed curves), as well as 2BF+TBF potentials (AV14+UIX and \tilde{v}_{14} +UIX) in LOCV and RLOCV frameworks (dashed and solid curves), respectively.

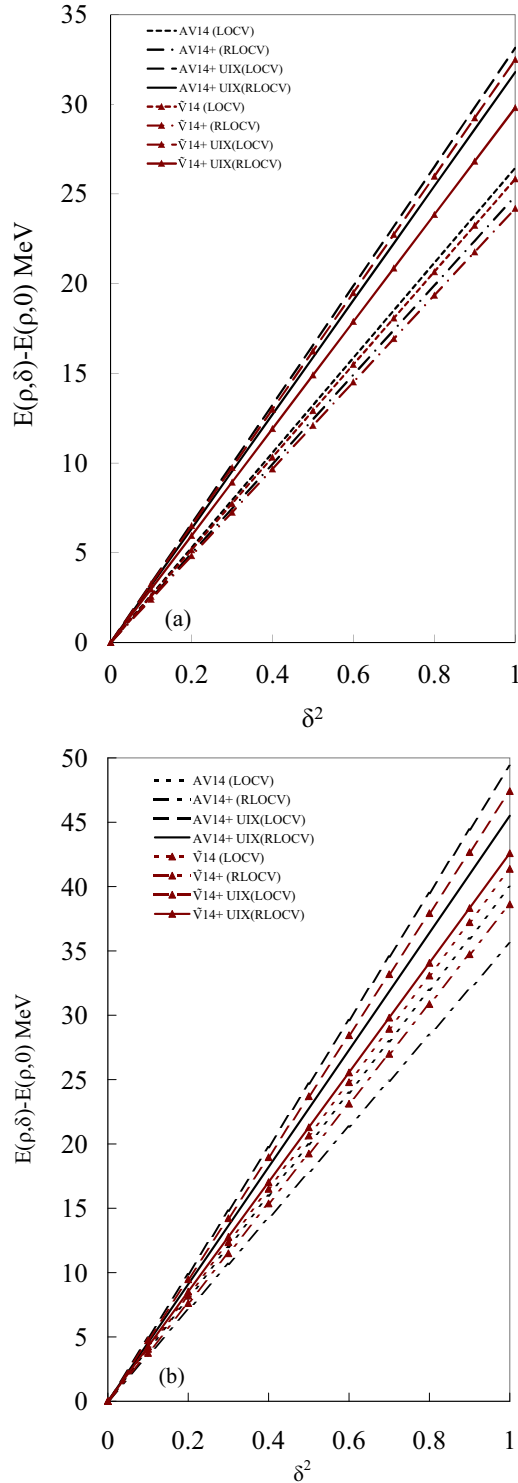


FIG. 5. (a) The LOCV and RLOCV calculations of the quadratic dependence of the nuclear symmetry energy as a function of δ^2 using two different versions of 2BF as well as 2BF+TBF interactions at $\rho = 0.17 \text{ fm}^{-3}$. (b) The same as (a) but at $\rho = 0.35 \text{ fm}^{-3}$.

and \tilde{v}_{14} +UIX. Figure 5(a) shows to the results at empirical saturation density (0.17 fm^{-3}) while Fig. 5(b) is devoted to the density (0.35 fm^{-3}). It is seen that in all cases the

symmetry energy increases nearly linearly with δ^2 . Therefore, the parabolic law is actually valid in the whole range of δ . The slope of each curve describes the approximate value of symmetry energy at the density (0.17 fm^{-3}). As can be seen from Fig. 5(a), the symmetry energy is almost independent of kind of potentials, namely nonrelativistic or relativistic ones. Furthermore, inclusion of RC has no noticeable effect on the curves and the value of symmetry energy, while TBF causes a remarkable difference on the curves and the value of symmetry energy compared with the case of using only 2BF. It can be seen from Fig. 5(b) that the effects of TBF and RC on the symmetry energy almost cancel each other specially in relativistic potential.

The exact and approximate values of nuclear symmetry energy of asymmetric nuclear matter can be calculated from Eqs. (5) and (6), respectively. The results of nuclear symmetry energy against density in both the LOCV and RLOCV calculations, with and without including TBF using AV14 and \tilde{v}_{14} , are shown in Fig. 6. Figure 6(a) shows the results obtained in the LOCV framework, while Fig. 6(b) is devoted to the results of the RLOCV treatment. It is observed from both panels that including TBF causes a remarkable difference in both value and behavior of $E_{\text{sym}}(\rho)$ in comparison with the case of using only 2BF. The calculations in both the LOCV and RLOCV approaches for both versions of potentials with and without including TBF provide the same values for symmetry energy at low densities, which tend to be different at higher ones. This is quite expected that the effects of RC become important at higher densities. These differences in the values of symmetry energy begin at high densities in the LOCV approach, while they start at moderate densities in the RLOCV approach. Moreover, using only 2BF interactions leads to a sharply increasing function of density, while including the TBF to both versions of potentials produces a symmetry energy with higher values at low and moderate densities tending to saturated at higher ones in both the LOCV and RLOCV formalisms. It can be seen from both panels that the effect of RC causes no significant differences in the value and particularly in the behavior of $E_{\text{sym}}(\rho)$ using two versions of potentials. The effect of RC on the value of $E_{\text{sym}}(\rho)$ is small at low densities, while this effect increases at higher densities, as expected. In addition, there is no important difference, especially between the common behavior and the values of $E_{\text{sym}}(\rho)$ calculated from approximate and exact relations. These results are in agreement with the calculation of the AV18 potential in Ref. [50].

In Fig. 7, the density dependence of symmetry energy calculated in the RLOCV method by using both relativistic and nonrelativistic versions of 2BF interactions as well as 2BF+TBF ones is compared with the other many-body calculations using different potentials, such as AP in the variational method with AV18 interaction [58], MB in the density-dependence Michigan three Yukawa terms (DDM3Y) model [59], GMH in the LOCV approach by using AV18 [50], MZE in the BHF approach with both AV18 and Bonn potentials [60], ZBLSZ in BHF by including TBF using AV18 [61] or LLSZ by using Bonn [55], and LKLB in DBHF with AV18 [53]. It is observed that the results obtained in the present work, around saturation density, and especially by

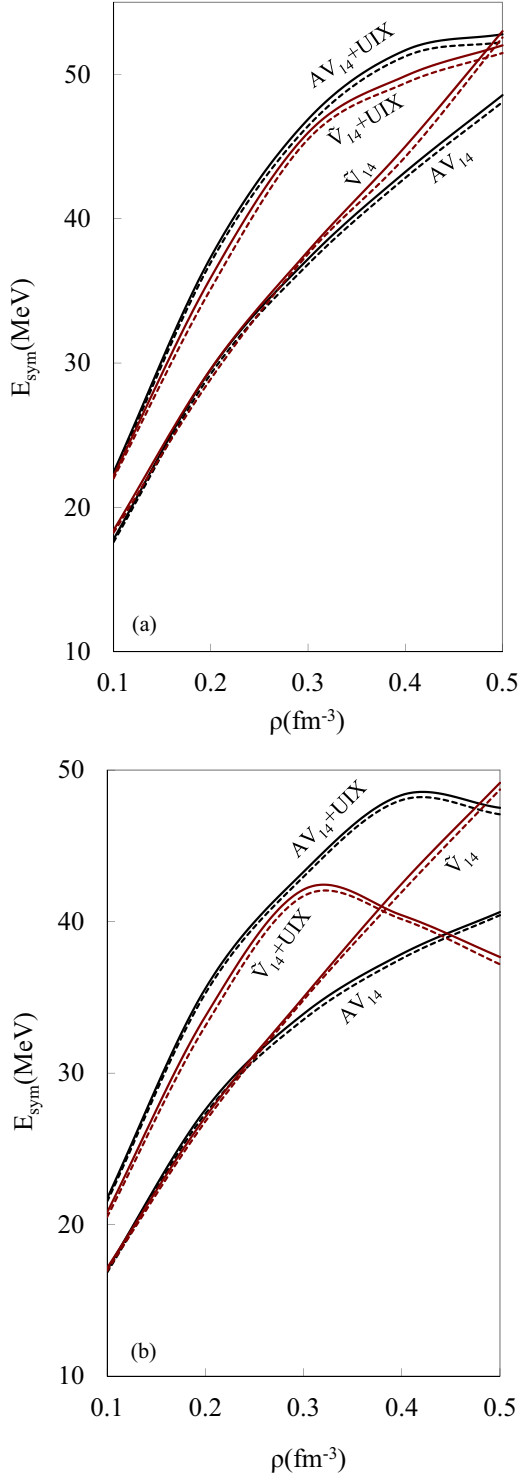


FIG. 6. (a) The exact (solid curves) and approximate (dashed curves) values of density dependence of symmetry energy obtained by LOCV approach for different potentials. (b) The same as panel (a) but for RLOCV approach.

including TBF, are in ordinary agreement with those extracted within other many-body methods.

The values of E_{sym} as well as its slope and curvature and K_{asy} calculated from our method are presented in Table V. It

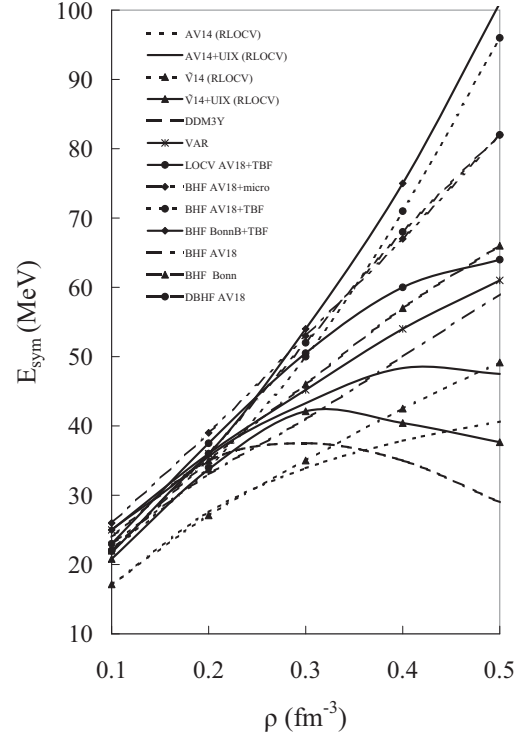


FIG. 7. The comparison of the nuclear symmetry energy against density calculated in this work with other potentials and many-body techniques.

can be seen that the value of $E_{\text{sym}}(\rho_0)$ in the LOCV method using nonrelativistic 2BF is 39.0 MeV, which is too large, while its relativistic version of 2BF in the LOCV method leads to the smaller value (34.9 MeV) for E_{sym} where none of them lie in the empirical range (31.6 ± 2.66) [62]. However, the calculations for the slope parameters at normal density predict the values 62.7 and 65.9 MeV for AV14 and \tilde{v}_{14} , respectively, which are both consistent with the range 58.9 ± 16.0 MeV [62]. The value of the isospin-dependent part of the incompressibility of SNM (K_{asy}) obtained by 2BF within the LOCV method is -513.7 (-467.9) MeV for AV14 (\tilde{v}_{14}), which both lie in the experimental range -550 ± 100 MeV [63]. The similar calculations within the RLOCV model show that both L and K_{asy} calculated by using \tilde{v}_{14} lie in the experimental ranges for these quantities which were mentioned earlier, while for AV14 it is not the case. Even though including TBF to \tilde{v}_{14} causes E_{sym} , L , and K_{asy} in the LOCV calculation lie in acceptable ranges, K_{asy} is not in the acceptable area for AV14. In the RLOCV treatment all of these values lie in the acceptable area for both AV14+UIX and \tilde{v}_{14} +UIX. It can be understood that the properties of nuclear matter such as binding energy, normal density, incompressibility, symmetry energy, etc., lie in the experimental area in the RLOCV approach using \tilde{v}_{14} +UIX.

We have separated the symmetry energy into its one-body $\langle E_1 \rangle$ and two-body $\langle E_2 \rangle$ energies parts. Our results at each saturation density (which are represented in Table I) are reported in Table VI. The first four columns are devoted to the LOCV approach and the next four columns present

TABLE V. The values of nuclear symmetry energy at saturation density, its slope and curvature and K_{asy} .

Potential (method)	E_{sym} (MeV)	L (MeV)	\mathcal{K}_{sym} (MeV)	\mathcal{K}_{asy} (MeV)
AV18 (LOCV) [37]	40.52	74.1	-76.3	-520.6
AV18+UIX (LOCV) [50]	34.17	77.3	-95.9	-559.9
AV18 (BHF) [8]	35.8	63.1	-27.8	-339.6
AV18+UIX (BHF) [8]	33.6	66.9	-23.4	-343.8
MDI (SHF) [67]	30.5	14.7	-264.0	-352.0
SLY4 (SHF) [67]	31.8	45.4	-119.9	-392.1
NL3 (RMF) [68]	37.29	118.2	100.9	-608.3
FSUGold (RMF) [69]	32.59	60.5	-51.3	-414.3
TM1 (RMF) [70]	36.9	110.8		
DDM3Y (RMF) [71]	30.71	45.11	-183.7	-454.4
AV14 (LOCV) (this work)	39.0	62.7	-137.6	-513.7
AV14 (RLOCV) (this work)	37.0	39.7	-196.8	-434.7
AV14+UIX (LOCV) (this work)	33.7	69.6	-234.7	-652.5
AV14+UIX (RLOCV) (this work)	33.3	60.8	-233.8	-598.6
\tilde{v}_{14} (LOCV) (this work)	34.9	65.9	-72.2	-467.9
\tilde{v}_{14} (RLOCV) (this work)	35.8	70.4	-71.8	-494.4
\tilde{v}_{14} +UIX (LOCV) (this work)	31.4	66.0	-187.8	-584.0
\tilde{v}_{14} +UIX (RLOCV) (this work)	30.3	60.1	-118.1	-478.7

RLOCV calculations. It is also seen from this table that the larger contribution of $E_{\text{sym}}(\rho_0)$ comes from the $\langle E_1 \rangle$ part compared to $\langle E_2 \rangle$ when only 2BF interactions are considered, while if TBF is included in our interactions, the contribution of the $\langle E_2 \rangle$ part in $E_{\text{sym}}(\rho_0)$ becomes more than $\langle E_1 \rangle$ in both LOCV and RLOCV approaches, as physically expected.

The partial wave decomposition of the $\langle E_2 \rangle$ part of $E_{\text{sym}}(\rho_0)$ up to $J = 2$ at each normal density (ρ_0) has been represented in Table VII. It is observed, in the RLOCV approach, that the absolute value of the separate contributions of each channel to E_{sym} are more than the LOCV approach for both 2BF and 2BF+TBF interactions. Also, by using 2BF+TBF, the absolute value of separate contributions of partial wave energies of each channel to E_{sym} are smaller in comparison to using only the 2BF interaction except 3S_1 - 3D_1 , which has the larger contribution to symmetry energy when TBF are added to 2BF interactions. The 3S_1 - 3D_1 channel gives the largest contribution to $E_{\text{sym}}(\rho_0)$ in all studied cases. Therefore, the spin triplet ($S = 1$) and isospin singlet ($T = 0$) channel contribute the most to symmetry energy. Similar results have been reported in Refs. [50,52], which indicates that the tensor component of the nuclear potential makes a significant contribution to symmetry energy. In addition, the absolute value of the contribution of each channel to sym-

metry energy for relativistic version of potential (\tilde{v}_{14}) is less than the nonrelativistic version whether 2BF or 2BF+TBF has been used in either the LOCV or RLOCV method. As mentioned, it is due to the fact that the tensor force component of \tilde{v}_{14} is less than the nonrelativistic version.

C. β -stable matter

The equilibrium configuration of β -stable matter (BSM) can be obtained at each total baryon number density (ρ_B) by minimizing the binding energy with respect to the two-body correlation functions and the relative proton abundance (ρ_p/ρ_B) subject to the constraints of Eqs. (10), (11), and (14) and the normalization constraint in LOCV or RLOCV calculations.

The EOS of BSM (without considering baryon rest masses) are plotted in Fig. 8 in both the LOCV and RLOCV frameworks with and without including TBF for both nonrelativistic and relativistic versions of interactions, i.e., AV14 and \tilde{v}_{14} . The results of PNM are also shown in Fig. 9 for comparison. It is seen that the extra degree of freedom presented by β decay leads to a softer EOS than the PNM. As expected, the BSM becomes harder by adding TBF to our interactions, while it becomes softer when RC is included in our calculations for both versions of potential. In other words, at a constant density, inclusion of RC decreases the binding energy per

TABLE VI. The contribution of one-body and two-body cluster energy in E_{sym} at each ρ_0 for two different versions of 2BF as well as 2BF+TBF interactions in both LOCV and RLOCV frameworks. All the quantities are in MeV.

	LOCV				RLOCV			
	AV14	\tilde{v}_{14}	AV14+UIX	\tilde{v}_{14} +UIX	AV14	\tilde{v}_{14}	AV14+UIX	\tilde{v}_{14} +UIX
$\langle E_1 \rangle$ (MeV)	20.74	17.31	13.22	12.69	22.74	19.23	13.70	13.54
$\langle E_2 \rangle$ (MeV)	17.62	15.72	19.23	18.18	18.52	17.50	19.28	19.32
Total (MeV)	38.36	33.03	32.46	30.87	41.25	36.73	33.68	32.86

TABLE VII. The separate contributions of partial wave energies of $\langle E_2 \rangle$ part of symmetry energy (in MeV) at each ρ_0 for two different versions of 2BF as well as 2BF+TBF interactions in both LOCV and RLOCV frameworks.

	LOCV				RLOCV			
	AV14	\tilde{v}_{14}	AV14+UIX	\tilde{v}_{14} +UIX	AV14	\tilde{v}_{14}	AV14+UIX	\tilde{v}_{14} +UIX
1S_0	2.22	1.47	0.60	0.58	3.08	2.29	0.83	0.98
3P_0	0.30	-0.031	0.0011	-0.097	0.69	0.33	0.081	0.043
1P_1	-7.94	-6.02	-5.51	-5.03	-9.34	-7.25	-6.01	-5.89
3S_1 - 3D_1	23.04	18.89	26.11	23.52	23.11	18.95	27.17	25.27
3P_1	6.79	5.17	4.11	3.56	8.23	6.52	4.41	4.11
1D_2	-4.95	-3.56	-2.81	-2.52	-5.78	-4.28	-3.04	-2.92
3D_2	9.44	6.83	2.56	2.30	11.13	8.31	2.76	2.64
3P_2 - 3F_2	-11.28	-7.03	-5.83	-4.14	-12.61	-7.36	-6.22	-4.92

nucleon while inclusion of TBF increases the binding energy and makes it more density dependent. Also, the effect of TBF is more significant on the EOS of BSM in compared to the effects of RC. Moreover, the EOS of BSM by using only 2BF relativistic version of potential (\tilde{v}_{14}) is harder than the nonrelativistic one (AV14) in both LOCV and RLOCV calculations. The same behavior is also observed for 2BF+TBF potentials (\tilde{v}_{14} +UIX, AV14+UIX). The EOS of BSM in relativistic and nonrelativistic approaches are not very different at low densities for both 2BF and 2BF+TBF interactions, but the results become different at high densities. Therefore, one can

conclude that in protonneutron stars which have high density, the effect of RC and particularly TBF may be very important in determining the EOS of these stars.

In Fig. 10 the energy per baryon number density of BSM has been plotted for both AV18 and its 2BF+TBF interaction (AV18+UIX) as a function of density. The results for PNM obtained by GMH [50] have been also represented for comparison. The effect of TBF on BSM for this potential is also very similar to the above-mentioned interactions.

The relative proton abundance (ρ_p/ρ_B) for relativistic and nonrelativistic approaches with and without including TBF in our interactions versus baryon density is plotted in Fig. 11. The results of the nonrelativistic version of potential (AV14) are plotted in Fig. 11(a) while Fig. 11(b) shows the results of the relativistic one (\tilde{v}_{14}). It can be seen from

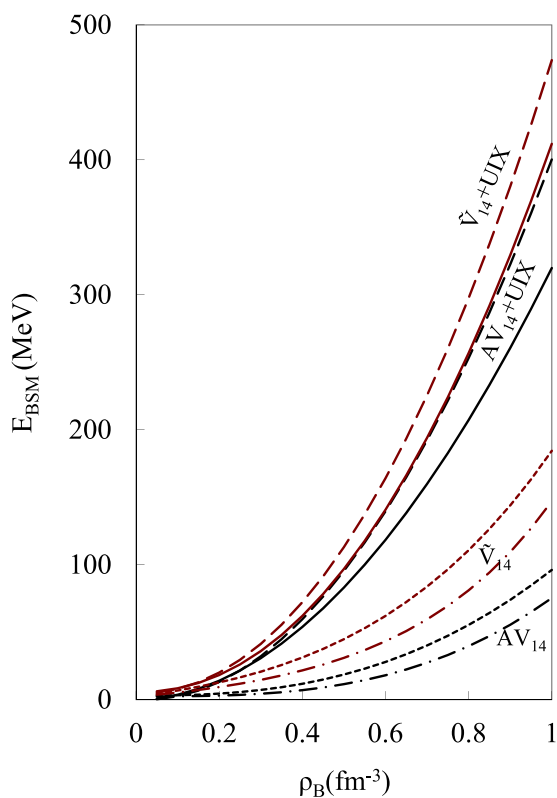


FIG. 8. The energy of BSM without considering baryon rest masses as a function of baryon densities. Dot (dot-dashed) curves represent our results for LOCV (RLOCV) calculation using only 2BF and dashed (solid) curves are used for LOCV (RLOCV) methods using 2BF+TBF.

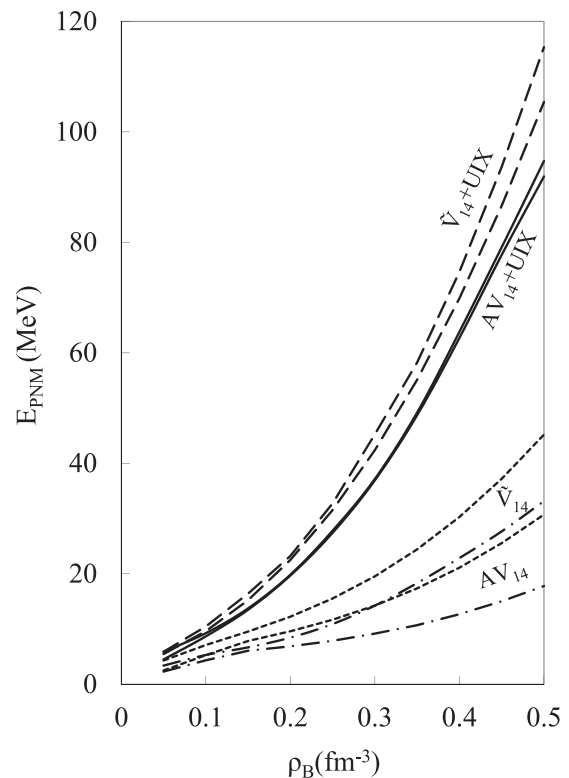


FIG. 9. The same as Fig. 8 but for PNM.

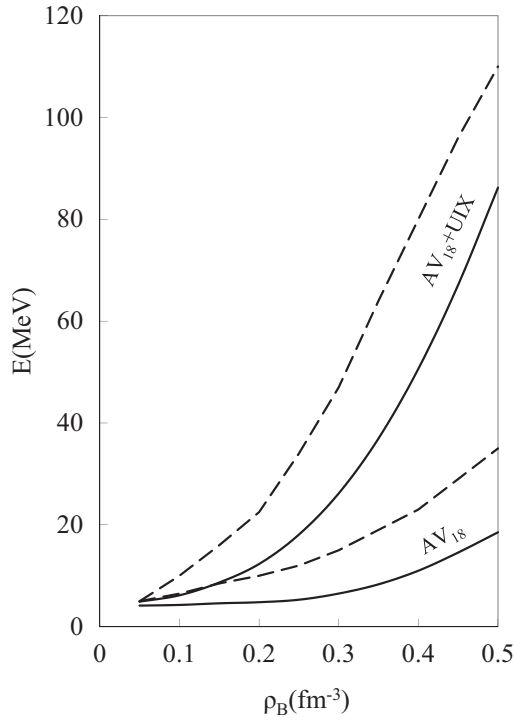


FIG. 10. The EOS of PNM as well as BSM using AV18 with and without including TBF. The solid curves represent the calculated EOS of BSM and broken curves show the results of PNM.

Fig. 11(a) that in LOCV calculations, by using only 2BF (AV14), the relative proton abundance increases by increasing baryon density which tends to be saturated at high densities

($\rho > 1 \text{ fm}^{-3}$), while including the RC provides ρ_p/ρ_B with lower values, which is saturated at the moderate density 0.35 fm^{-3} . It reaches 4% of the baryon abundance. On the other hand, adding TBF to our interaction produces the relative proton abundance with higher values at low densities, which is saturated at the same density (0.35 fm^{-3}) in LOCV as well as in RLOCV frameworks. By using AV14+UIX, this ratio comes to 8.5% of the baryon abundance in LOCV treatment, while reaching 6% of the baryon density in the RLOCV method. Therefore, adding RC to the β -stable results decreases the maximum ρ_p/ρ_B , while including TBF increases the maximum value of proton abundance. It is observed that Fig. 11(b) has similar behaviors by including RC as well as TBF in the β -stable results. By using relativistic potential \tilde{v}_{14} , the maximum of the proton abundance is pushed to the higher baryon densities with the lower proton abundance with respect to the nonrelativistic version. If only the 2BF interaction \tilde{v}_{14} uses the LOCV (RLOCV) calculation, then the maximum value of proton abundance is 3% (1.8%) of the baryon density, which occurs at baryon density 0.8 fm^{-3} . By adding TBF, the value ρ_p/ρ_B is pushed to the lower baryon densities. The maximum of proton abundance is around 6.4% (5.3%) of baryon abundance at the baryon number density 0.35 fm^{-3} for the LOCV (RLOCV) formalism. So the maximum value of proton abundance depends on the relativistic or nonrelativistic versions of interaction, and the relativistic or nonrelativistic approach, and particularly on the TBF. Since in protoneutron stars we deal with dense matter at high energies, the effects of RC as well as TBF may be very important on the maximum of proton abundance. Moreover, it can be concluded that using

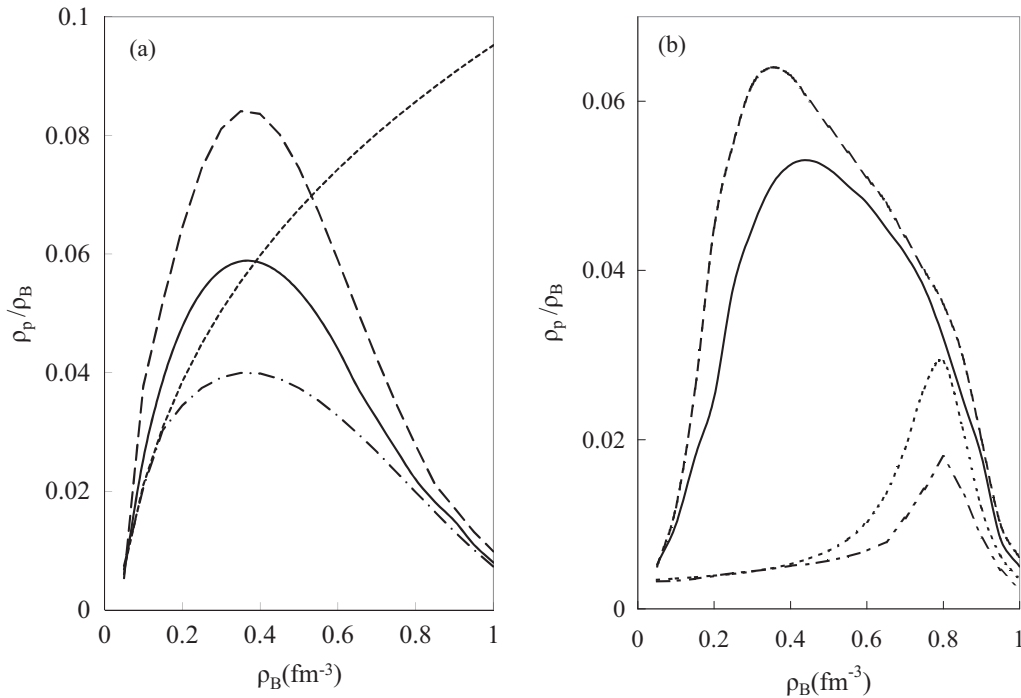


FIG. 11. (a) The comparison of the relative proton abundance against baryon number density using AV14. Dot (dot-dashed) curves show the results by using 2BF in LOCV (RLOCV) treatment and dashed (solid) curves show the results by using 2BF+TBF in these approaches, respectively. (b) The same as panel (a) but for \tilde{v}_{14} .

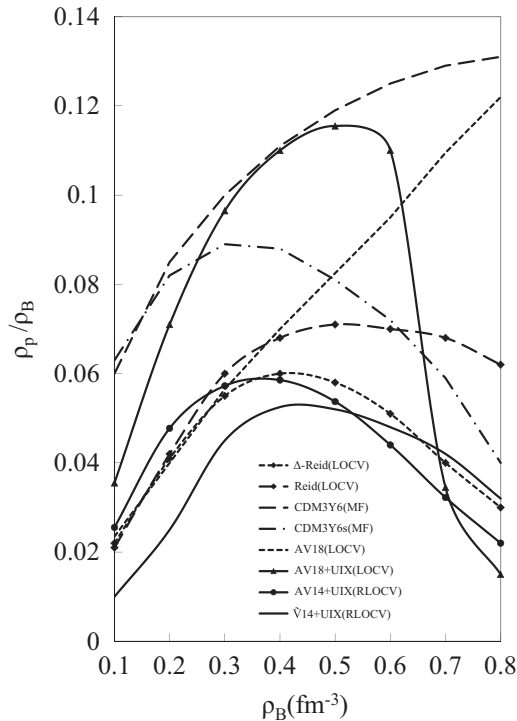


FIG. 12. The proton abundance ρ_p/ρ_B as a function of baryon density calculated in this work as well as other methods and interactions.

the realistic potential which has been fitted relativistically to nucleon-nucleon scattering phase shifts may affect the maximum of proton abundance. This shows that, aside from

particles densities, the RC, and in particular the TBF, may play a great role in the EOS of neutron stars.

The proton abundance ρ_p/ρ_B calculated by using AV18 and AV18+UIX is also shown in Fig. 12. Similar results with mentioned potentials are observed when TBF includes the AV18 interaction. So it can be concluded that using 2BF+TBF interactions, the protoneutron stars may have a higher ρ_p at lower densities, with respect to using only the 2BF interaction. The results of MM [48] in the LOCV formalism with Reid and Δ -Reid interactions and TLKM [12] in a mean-field study with CDM3Y6 and CDM3Y6s interactions are also presented for comparison. The agreement is good, particularly at low-baryon-number densities. The quantity ρ_p/ρ_B , which is obtained by employing 2BF interactions AV14 and AV18 in the present work and those calculated by TLKM with CDM3Y6 interaction increase, while the results using 2BF+TBF potentials AV18+UIX, AV14+UIX and those of MM with Reid and Δ -Reid and TLKM with CDM3Y6s show a decreasing trend in relative proton abundance.

The maximum of relative proton abundance is due to the fact that in the above interactions, the system takes advantage of the tensor components. Since the 2BF+UIX (TBF) interaction has more repulsive components compared with 2BF, such as the 3S_1 - 3D_1 channel, the peak consequently occurs at a lower density.

In Fig. 13 the calculated number densities of protons (p), electrons (e), and muons (μ) have been plotted as a function of the total baryon number density in both nonrelativistic and relativistic treatment for both 2BF and 2BF+TBF interactions. The results of AV₁₄, \tilde{v}_{14} , and AV18 have been shown in Figs. 13(a), 13(b), and 13(c), respectively. We find that ρ_p , ρ_e , and ρ_μ increase (decrease) by including TBF in

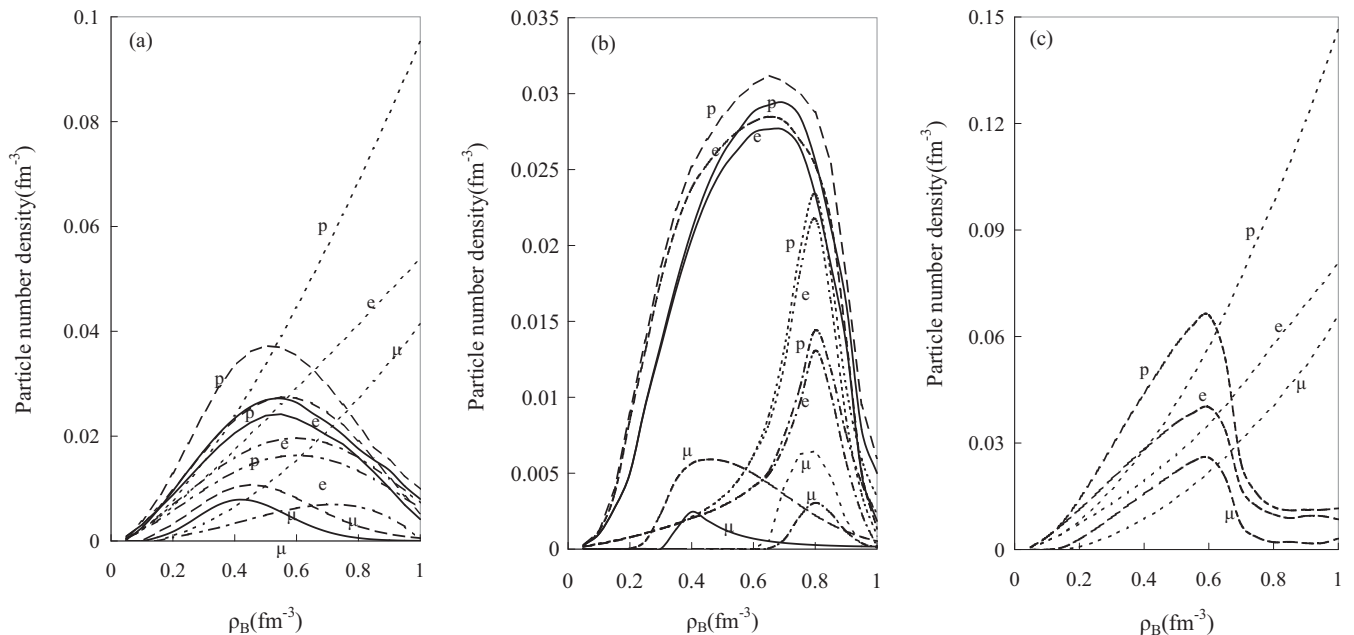


FIG. 13. (a) The particle densities of proton, electron and muon versus baryon density, for AV14 potentials with and without adding TBF to our interactions in both RLOCV (solid and dot-dashed curves) and LOCV (dashed and dot curves) frameworks. (b) The same as panel (a) but for \tilde{v}_{14} . (c) The same as panel (a) but for AV18 only in LOCV method.

low (high) baryonic densities. It is also seen from Fig. 13(a) that the muon densities are almost zero for $\rho_B \leq 0.15 \text{ fm}^{-3}$ in the LOCV framework using the 2BF interaction AV14, and the muons set in at higher baryon density as we include RC to our calculations, while they begin at lower baryon number density when TBF are included in our interactions. These effects are much more pronounced in the case of the \tilde{v}_{14} potential. So the muon densities get started for $\rho_B \geq 0.6 \text{ fm}^{-3}$ in the LOCV framework by using the 2BF \tilde{v}_{14} interaction and the muons set in at lower baryon number density when TBF is added to the \tilde{v}_{14} interaction. This shows that the effect of RC on particle densities is the opposite of the effect of TBF. A similar behavior happens for 2BF AV18 and its 2BF+TBF interaction (AV18+UIX), as shown in Fig. 13(c). Like AV14, using the 2BF potential, the muon's densities set in at $\rho_B = 0.15 \text{ fm}^{-3}$, which leads to lower baryonic densities when the 2BF+TBF interaction is used.

VII. SUMMARY AND CONCLUSION

In summary, the LOCV approach with the inclusion of RC as well as TBF of the Urbana UIX interaction is used to study the properties of cold nuclear matter, with the focus on the roles of RC and TBF on the properties of such nucleonic matter. In order to compare the relativistic effects with the effects of TBF, we have used two different versions of v_{14} , relativistic (\tilde{v}_{14}) and nonrelativistic (AV14) ones, as the bare two-body interactions. The separate contributions of RC as well as TBF of partial wave energies are also calculated. It is found that the 1S_0 partial wave provides the largest contribution of relativistic effects for both versions of interactions, while the major contribution to the effects TBF come through the 3S_1 - 3D_1 channel.

The values of binding energy, saturation density in a wide range of asymmetry parameters, incompressibility, symmetry energy and its slope and curvature parameters, and the density dependence of nuclear symmetry energy are also investigated. It can be concluded that with the inclusion of TBF to the relativistic lowest-order constrained variation formalism, the RLOCV is successful to reproduce correctly the nuclear matter saturation properties, i.e., density, binding energy, the isobaric incompressibility at saturation point, as well as the symmetry energy and its slope and curvature. Most of the mentioned quantities lie in the experimental ranges by using AV14, while all of them lie within the experimentally determined ranges by using \tilde{v}_{14} . It is also found that the coupled channel 3S_1 - 3D_1 provides the largest contribution to symmetry energy.

The β -stable matter and its proton abundance in a wide range of baryon number densities are also studied. It is seen that the extra degree of freedom offered by the β decay leads to a slight softening of EOS, as would be expected. It is seen that the maximum values of proton abundance which are obtained by 2BF+3BF interactions are much larger than those of 2BF potentials (AV₁₄, \tilde{v}_{14} , AV18) and they occurred in much lower baryon number densities. It was observed that adding RC to our calculations has an opposite effect on BSM with respect to the effect of TBF. It was shown that the RC and especially TBF may play an important role in increasing

the percentage of proton abundance in proton-neutron stars. In the central core of these stars, which is so dense, the role of TBF can be great, and these stars may have lower densities than previously thought. The EOS of BSM is softer than PNM and the effects of RC and TBF may influence the structure of nucleonic stars and the behavior of dense matter.

In conclusion, despite close agreements between the results of the LOCV method and other many-body techniques, i.e., BHF, FHNC, etc., it is worthwhile to mention that the correlation function is a key quantity to characterize each many-body method. The short- and long-range correlation functions are directly available in the LOCV method, while in the BHF framework the short-range correlation functions can extract only through defect function. This fact has been elucidated in Ref. [40]. In the LOCV method, the average kinetic energy is affected directly by correlations, and the total correlation energy includes a kinetic part and a potential part. But in the BHF scheme the kinetic energy is not modified and the whole correlation energy is contained in the potential part extracted from the G matrix, which describes the two-nucleon scattering amplitude. On the other hand the kinetic energy in BHF framework modifies by the momentum dependence of G matrix [40]. The LOCV formalism is a fully self-consistent method with state-dependent correlation functions. There is no free parameter in this approach, except those included in the potentials. The only constraint that is considered in the LOCV formalism is the normalization condition, which is the physical condition of the system. This assumption keeps the higher-order terms as small as possible. By functionally minimizing the two-body energy with respect to the short-range parts of the correlation functions, we obtained a set of Euler-Lagrange equations. The long-range behavior of the correlation functions also assumes a particular form in order to carry out an exact functional minimization. The functional minimization procedure represents a great computational simplification over the unconstrained methods such as VHC, where the short-range behavior of the correlation functions is parameterized, trying to go beyond the lowest order. In other microscopic methods, such as the BHF approach, only the expectation value of the energy is obtained without calculating any correlation functions.

The correlation functions are very important in calculating two-nucleon spectral functions. These functions contain information on the NN correlations, the nuclear structure, and, in particular, the NN interactions. The spectral functions of the many-body systems can give us important quantities, such as the one-particle ground-state energy. Moreover, by calculating the spectral function of a nucleus, it can extract the correlation energy between the two nucleons and eventually find the total ground-state energy of the system. Thus, as was pointed out, the calculation of the two-proton spectral functions of a nucleus is an important quantity of interest. In recent years, generally a number of theoretical methods have been carried out for determining the two-nucleon spectral functions with different approximations. In these works the short-range correlation and the long-range effects have been able to closely explain the experimental properties of the target ground state. However, the connection of the correlation function and the spectral function is very transparent in the

LOCV method [72], while it is not straightforward in BHF [73]. Finally, another advantage of the LOCV framework is that not only can it apply for whole densities (from lower to higher than the saturation point) but also it has been extended to the relativistic approach, it can be added to TBF, and it can be used at finite temperature.

So, with respect to the above arguments, one can conclude that most of the minor differences in the results of LOCV and other variational methods return to density behavior of correlations functions, which is discussed in the appropriate references. Thus, we can claim the LOCV is a good candidate to approximate nuclear symmetry energy and its density dependence as well as the proton abundance of β -stable matter.

-
- [1] G. F. Bertsch and S. Das Gupta, *Phys. Rep.* **160**, 189 (1988).
- [2] M. Prakash, I. Bombaci, P. J. Ellis, R. Knorren, and J. M. Lattimar, *Phys. Rep.* **280**, 1 (1997).
- [3] I. Bombaci, T. T. S. Kuo, and U. Lombardo, *Phys. Rep.* **242**, 165 (1994).
- [4] B. A. Li and L. W. Chen, *Phys. Rev. C* **72**, 064611 (2005).
- [5] B. A. Brown, *Phys. Rev. Lett.* **85**, 5296 (2000).
- [6] S. Typel and B. A. Brown, *Phys. Rev. C* **64**, 027302 (2001).
- [7] J. Lattimer and M. Prakash, *Astrophys. J.* **550**, 426 (2001).
- [8] I. Vidaña, C. Providência, A. Polls, and A. Rios, *Phys. Rev. C* **80**, 045806 (2009).
- [9] J. L. Friar, *Phys. Rev. C* **12**, 695 (1975).
- [10] W. Zuo *et al.*, *Phys. Lett. B* **595**, 44 (2004).
- [11] Ch. C. Moustakidis, *Phys. Rev. C* **78**, 054323 (2008).
- [12] N. H. Tan, D. T. Loan, D. T. Khoa, and J. Margueron, *Phys. Rev. C* **93**, 035806 (2016).
- [13] M. Farine, J. M. Person, and B. Rouben, *Nucl. Phys. A* **304**, 317 (1978).
- [14] J. M. Person *et al.*, *Nucl. Phys. A* **528**, 1 (1991).
- [15] B. D. Serot and J. D. Walecka, *Advances in Nuclear Physics*, Vol. 16 (Plenum Press, 1986), pp. 1–327.
- [16] M. Baldo, G. Giansiracusa, U. Lombardo, and H. Q. Song, *Phys. Lett. B* **473**, 1 (2000).
- [17] I. E. Lagaris and V. R. Pandharipande, *Nucl. Phys. A* **359**, 331 (1981).
- [18] S. Moroni, S. Fantoni, and G. Senatore, *Phys. Rev. B* **52**, 13547 (1995).
- [19] J. C. Owen, R. F. Bishop, and J. M. Irvine, *Nucl. Phys. A* **277**, 45 (1977).
- [20] R. V. Reid, *Ann. Phys. (NY)* **50**, 411 (1967).
- [21] A. M. Green, J. A. Niskanen, and M. E. Sainio, *J. Phys. G: Nucl. Part. Phys.* **4**, 1055 (1978).
- [22] R. B. Wiringa, R. A. Smith, and T. L. Ainsworth, *Phys. Rev. C* **29**, 1207 (1984).
- [23] R. B. Wiringa, V. G. J. Stoks, and R. Schiavilla, *Phys. Rev. C* **51**, 38 (1995).
- [24] J. Carlson and V. R. Pandharipande and R. Schiavilla, *Phys. Rev. C* **47**, 484 (1993).
- [25] J. L. Forest, V. R. Pandharipande, J. Carlson, and R. Schiavilla, *Phys. Rev. C* **52**, 576 (1995).
- [26] H. R. Moshfegh and M. Modarres, *Nucl. Phys. A* **749**, 130 (2005).
- [27] H. R. Moshfegh and M. Modarres, *Nucl. Phys. A* **792**, 201 (2007).
- [28] H. R. Moshfegh and M. Modarres, *Nucl. Phys. A* **759**, 79 (2005).
- [29] S. Zaryouni, *Nucl. Phys. A* **834**, 564c (2010).
- [30] S. Zaryouni and H. R. Moshfegh, *Int. J. Mod. Phys. E* **14**, 297 (2005).
- [31] B. Bakamjian and L. H. Thomas, *Phys. Rev.* **92**, 1300 (1952).
- [32] R. A. Krajcik and L. L. Foldy, *Phys. Rev. D* **10**, 1777 (1974).
- [33] A. Akmal, V. R. Pandharipande, and D. G. Ravenhall, *Phys. Rev. C* **58**, 1804 (1998).
- [34] H. R. Moshfegh and S. Zaryouni, *Eur. Phys. J. A* **43**, 284 (2010).
- [35] S. Zaryouni and H. R. Moshfegh, *Eur. Phys. J. A* **45**, 69 (2010).
- [36] S. Zaryouni, M. Hassani, and H. R. Moshfegh, *Phys. Rev. C* **89**, 014332 (2014).
- [37] G. E. Brown, W. Weise, G. Baym, and J. Speth, *Comm. Nucl. Part. Phys.* **17**, 39 (1987).
- [38] J. Carlson, V. R. Pandharipande, and R. B. Wiringa, *Nucl. Phys. A* **401**, 59 (1983).
- [39] S. Goudarzi and H. R. Moshfegh, *Phys. Rev. C* **91**, 054320 (2015).
- [40] M. Baldo and H. R. Moshfegh, *Phys. Rev. C* **86**, 024306 (2012).
- [41] B. S. Pudliner, V. R. Pandharipande, J. Carlson, S. C. Pieper, and R. B. Wiringa, *Phys. Rev. C* **56**, 1720 (1997).
- [42] B. S. Pudliner, V. R. Pandharipande, J. Carlson, and R. B. Wiringa, *Phys. Rev. Lett.* **74**, 4396 (1995).
- [43] S. C. Pieper, V. R. Pandharipande, R. B. Wiringa, and J. Carlson, *Phys. Rev. C* **64**, 014001 (2001).
- [44] E. Khan and J. Margueron, *Phys. Rev. C* **88**, 034319 (2013).
- [45] J. R. Stone, N. J. Stone, and S. A. Moszkowski, *Phys. Rev. C* **89**, 044316 (2014).
- [46] I. Bombaci and U. Lombardo, *Phys. Rev. C* **44**, 1892 (1991).
- [47] C. Howes, R. F. Bishop, and J. M. Irvine, *J. Phys. G: Nucl. Phys.* **4**, L123 (1978).
- [48] M. Modarres and H. R. Moshfegh, *Phys. Rev. C* **62**, 044308 (2000).
- [49] J. L. Forest, V. R. Pandharipande, and J. L. Friar, *Phys. Rev. C* **52**, 568 (1995).
- [50] S. Goudarzi, H. R. Moshfegh, and P. Haensel, *Nucl. Phys. A* **969**, 206 (2018).
- [51] L. Engvik *et al.*, *Astrophys. J.* **469**, 794 (1996).
- [52] I. Vidana, A. Polls, and C. Providencia, *Phys. Rev. C* **84**, 062801(R) (2011).
- [53] C.-H. Lee, T. T. S. Kuo, G. Q. Li, and G. E. Brown, *Phys. Rev. C* **57**, 3488 (1998).
- [54] D. Alonso and F. Sammarruca, *Phys. Rev. C* **67**, 054301 (2003).
- [55] Z. H. Li, U. Lombardo, H. J. Schulze, and W. Zuo, *Phys. Rev. C* **77**, 034316 (2008).
- [56] W. D. Myers and W. J. Swiatecki, *Phys. Rev. C* **57**, 3020 (1998).
- [57] H. R. Moshfegh and M. M. Ghazanfari, *J. Phys. G: Nucl. Part. Phys.* **38**, 085102 (2011).
- [58] A. Akmal and V. R. Pandharipande, *Phys. Rev. C* **56**, 2261 (1997).
- [59] T. K. Mukhopadhyay and D. N. Basu, *Nucl. Phys. A* **789**, 201 (2007).
- [60] H. M. M. Mansour, M. El-Zohry, and A. E. Elmeshneb, *Armenian J. Phys.* **11**, 1 (2018).

- [61] X. R. Zhou, G. F. Burgio, U. Lombardo, H. J. Schulze, and W. Zuo, *Phys. Rev. C* **69**, 018801 (2004).
- [62] B. A. Li and X. Han, *Phys. Lett. B* **727**, 276 (2013).
- [63] T. Li *et al.*, *Phys. Rev. Lett.* **99**, 162503 (2007).
- [64] R. B. Wiringa, V. Fiks, and A. Fabrocini, *Phys. Rev. C* **38**, 1010 (1988).
- [65] W. Zuo, A. Lejeune, U. Lombardo, and J. F. Mathiot, *Nucl. Phys. A* **706**, 418 (2002).
- [66] E. N. E. van Dalen, C. Fuchs, and A. Faessler, *Nucl. Phys. A* **744**, 227 (2004).
- [67] L. W. Chen, B. J. Cai, C. M. Ko, B. A. Li, C. Shen, and J. Xu, *Phys. Rev. C* **80**, 014322 (2009).
- [68] J. Piekarewicz and M. Centelles, *Phys. Rev. C* **79**, 054311 (2009).
- [69] B. G. Todd-Rutel and J. Piekarewicz, *Phys. Rev. Lett.* **95**, 122501 (2005).
- [70] Z. W. Zhang, S. S. Bao, J. N. Hu, and H. Shen, *Phys. Rev. C* **90**, 054302 (2014).
- [71] D. N. Basu, P. R. Chowdhury, and C. Samanta, *Phys. Rev. C* **80**, 057304 (2009).
- [72] M. Moddarres and Y. Younesizadeh, *Phys. Rev. C* **85**, 054305 (2012).
- [73] M. Baldo, M. Borromeo, and C. Ciofi degli, *Nucl. Phys. A* **604**, 429 (1996).